

TIME-DEPENDENT DENSITY DIAGNOSTICS OF SOLAR FLARE PLASMAS USING SDO/EVE

RYAN O. MILLIGAN¹, MICHAEL B. KENNEDY¹, MIHALIS MATHIOUDAKIS¹, & FRANCIS P. KEENAN¹

Draft version May 30, 2022

ABSTRACT

Temporally-resolved electron density measurements of solar flare plasmas are presented using data from the EUV Variability Experiment (EVE) onboard the Solar Dynamics Observatory (SDO). The EVE spectral range contains emission lines formed between 10^4 – 10^7 K, including transitions from highly ionized iron ($\gtrsim 10$ MK). Using three density-sensitive Fe XXI ratios, peak electron densities of $10^{11.2}$ – $10^{12.1}$ cm^{-3} were found during four X-class flares. While previous measurements of densities at such high temperatures were made at only one point during a flaring event, EVE now allows the temporal evolution of these high-temperature densities to be determined at 10 s cadence. A comparison with GOES data revealed that the peak of the density time profiles for each line ratio correlated well with that of the emission measure time profile for each of the events studied.

Subject headings: Sun: activity — Sun: corona — Sun: flares — Sun: UV radiation

1. INTRODUCTION

Solar flares are generally considered as increases in the X-ray luminosity on the Sun due to changes in the temperature and density of the coronal plasma. The increase in temperature is readily inferred from the presence of high-temperature ($\gtrsim 10$ MK) emission lines in solar flare spectra. However, precise values of the coronal electron density (N_e) have been more difficult to ascertain. Quite often these densities are estimated from broadband continuum measurements which can yield values of the flare emission measure ($EM = f \int_V N_e^2 dV$). Deconvolving density values from the emission measure requires a knowledge of the volume of the emitting plasma (V , estimated from imaging data) and a possible filling factor (f , usually assumed to be unity). Accurate measurements of the electron density are important for understanding both the heating and cooling of flare plasmas, and determining the mechanisms responsible.

A more reliable derivation of electron densities can be made using density-sensitive line ratios, which do not require prior knowledge of the emitting volume nor the filling factor, under the assumption that one of the lines arises from a metastable level. While there have been many studies that have presented the density structure of active regions at coronal temperatures (~ 1 – 2 MK; Gallagher et al. 2001, Warren & Winebarger 2003, Milligan et al. 2005) there have been fewer of the coronal plasma density during flares. McKenzie et al. (1980) and Doschek et al. (1981) used data from the SOLEX instrument onboard P78-1 to derive time-dependent flare densities from an O VII ratio (2 MK) and found that values reached a maximum of $\sim 10^{12}$ cm^{-3} at the peak of the impulsive phase. More recently, Milligan (2011) and Graham et al. (2011) measured electron densities of 10^{11} – 10^{12} cm^{-3} at flare footpoints during their impulsive phases from Fe XII (1.4 MK), Fe XIII (1.6 MK) and Fe XIV (1.8 MK) line ratios using data obtained from the EUV Imaging Spectrometer (EIS; Culhane et al.

2007) onboard Hinode. Warren et al. (2008) identified several Ca XV line pairs (formed at 4 MK) in the EIS wavelength range which are sensitive to densities in the range 10^9 – 10^{11} cm^{-3} , while Feldman et al. (2008) identified Ti, Cr, and Mn lines formed above 10 MK which are sensitive to densities from 10^{10} – 10^{13} cm^{-3} . However, due to the telemetry and planning restrictions implemented on Hinode observations, flare data from these lines are unlikely to become available.

Density diagnostics of flaring plasma using emission lines formed above ~ 10 MK have been even more elusive in recent decades. Among the first to identify such lines were Kastner et al. (1974) using data from the Goddard Space Flight Center (GSFC) scanning spectrograph onboard the Orbiting Solar Observatory (OSO)-5 satellite. These transitions were primarily from Fe XIX–Fe XXIII and found in the 9–14.5 nm portion of the EUV spectrum. Following Doschek et al. (1973), Mason et al. (1979) identified several Fe XXI line pairs in this wavelength range that could serve as density diagnostics during flares for values of N_e between 10^{11} – 10^{15} cm^{-3} . A preliminary application to OSO-5 data yielded typical flare densities $< 10^{13}$ cm^{-3} for temperatures ~ 10 MK. Mason et al. (1984) later refined these values, finding 4×10^{11} cm^{-3} for temperatures between $10^{6.5}$ and $10^{7.2}$ K. A similar detailed study of electron densities by Lawson & Peacock (1984) using the OSO-5 solar flare spectra found inconsistent values of $10^{12.8}$, $10^{11.7}$ and $10^{13.1}$ cm^{-3} from Fe XX, Fe XXI, and Fe XXII line ratios, respectively. However, the OSO-5 instrument took 2.5 minutes to scan the 9–14.5 nm wavelength range, meaning that each of the lines in a given ratio were recorded at different times, during which the flare was likely to have evolved. The instrument sensitivity as a function of wavelength was also uncertain.

Density diagnostics with improved spectral and temporal resolution were later obtained from the Bent Crystal Spectrometer (BCS) onboard the Solar Maximum Mission. This was a soft X-ray spectrometer that obtained high-resolution spectra in small wavelength intervals near 0.19 and 0.31 nm. An analysis of Fe XX lines in BCS spectra was performed by Phillips et al.

¹ Astrophysics Research Centre, School of Mathematics & Physics, Queen's University Belfast, University Road, Belfast, Northern Ireland, BT7 1NN

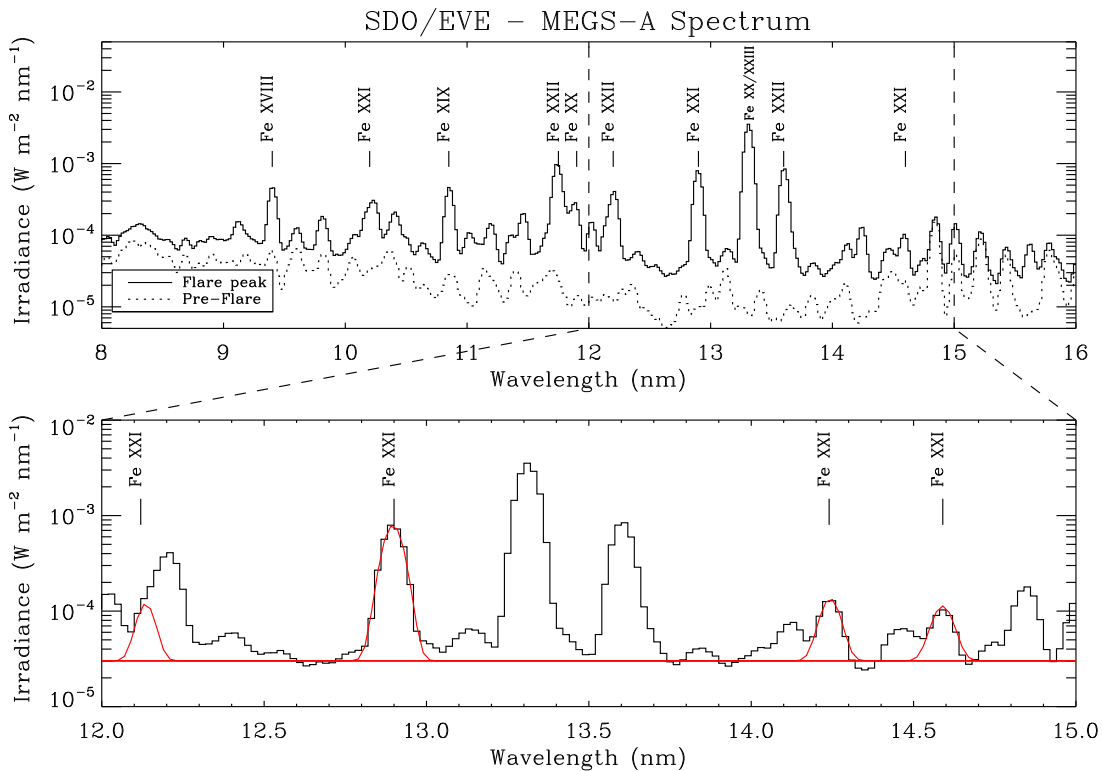


FIG. 1.— Top panel: The 8–16 nm portion of the EVE spectrum showing the presence of high-temperature Fe lines (XVIII–XXIII) at the peak of the X6.9 flare that occurred on 2011 August 9 (solid line), and from a quiescent time before the flare (dotted line). Bottom panel: Expanded view of the 12–15 nm range which contains the four Fe XXI lines used in this study. Overplotted are the fits to each of the lines as well as the background level, indicated by the horizontal line.

(1983) to obtain electron density values. In most cases values of the electron density were found to be $\sim 10^{11} \text{ cm}^{-3}$ and were therefore indistinguishable from the low density limit. However, there has been one report of solar flare densities as high as 10^{13} cm^{-3} from Fe XXII line ratios by Phillips et al. (1996). In the stellar case, observations made with the Extreme Ultraviolet Explorer also revealed coronal electron densities as high as 10^{13} cm^{-3} during the most energetic events (Monsignori Fossi et al. 1996). Coronal electron densities of this magnitude, if confirmed, could have significant implications for flare physics.

Earlier studies of flare densities using high-temperature line ratio techniques have each focused on a single time interval during the flare, often with an integration time of several minutes. Any time-resolved investigations were undertaken using lines formed at quiescent coronal temperatures. Here we present time profiles of electron density, determined using line ratios with formation temperatures in excess of 10 MK obtained using data from the EUV Variability Experiment (EVE; Woods et al. 2010) instrument onboard the Solar Dynamics Observatory (SDO). Section 2 gives an overview of the EVE instrument, the emission lines within the spectral range under consideration and a description of the methods used to analyse the data. In Section 3 we present results obtained from four X-class flares, while Section 4 summarizes the results and conclusions, and discusses the implications.

2. EVE OBSERVATIONS AND DATA ANALYSIS

EVE acquires full-disk (Sun-as-a-star) EUV spectra every 10 seconds over the 6.5–37 nm wavelength range us-

ing its MEGS-A (Multiple EUV Grating Spectrograph) component with a near 100% duty cycle. The 9–16 nm portion of this wavelength range contains many emission lines from transitions in high-temperature ($\gtrsim 10$ MK) Fe ions (XVIII–XXIII), as shown in the top panel of Figure 1. These high-temperature iron lines dominate the EVE spectrum during a flare (see Chamberlin et al. 2012).

Although the 9–16 nm range includes several species of high-temperature Fe lines, its coarse resolution (~ 0.1 nm) means that many of the observed line profiles were blended with other emission lines, or were too weak to be detected above the level of continuum emission. After investigating all possible density-sensitive line pairs for Fe XIX–XXII listed in Phillips et al. (2008; page 171, Figure 6.7), only three pairs of Fe XXI lines were deemed to be reliable (see bottom panel of Figure 1). These agree with those identified by Mason et al. (1979; 1984) and will be discussed in more detail in Section 2.1.

The identification of the emission lines present in the EVE spectra was performed by visually comparing the central wavelength of the observed emission features with the CHIANTI (version 7; Landi et al. 2012) line list. Synthetic line profiles for this list were generated using the ionization equilibrium files of Bryans et al. (2009), the flare DEM of Dere & Cook (1979), coronal abundances (Feldman et al. 1992), initial densities of 10^{11} and 10^{12} cm^{-3} , and at the EVE spectral bin size of 0.02 nm.

2.1. Fe XXI lines

The strongest Fe XXI emission line in the wavelength range studied is that at 12.875 nm (see also Mason et al. 1984). This is unblended and common to several density-sensitive line pairs, specifically 12.121/12.875, 14.214/12.875, and 14.573/12.875 (see Figure 2). The electron density of the flare plasma can be determined directly from the ratio of the peak intensities. For each density-sensitive line pair, the flux ratio as a function of N_e at the temperature of maximum ionisation fraction, which is ~ 12 MK for Fe XXI (Bryans et al. 2009), was calculated using CHIANTI. Lines were fitted with a Gaussian function and the peak, rather than integrated, flux used to calculate the ratio values from which the densities were derived. This was to avoid including any potential weaker line emission in the wings of the feature of interest to the total line flux.

The Fe XXI line at 14.214 nm is blended with another Fe XXI transition at 14.228 nm, and was observed as a single emission feature due to their central wavelengths being separated by only 0.014 nm, which is within one wavelength bin of the EVE spectra. Therefore, the density-sensitive ratio was determined from the sum of the flux of these two lines. This results in the (14.214+14.228)/12.875 ratio being less sensitive to lower densities than if the lines were resolved (dotted line in Figure 2).

The 12.121 nm line was weak in many cases and is blended in the blue wing of Fe XX 12.184 nm but is involved in a ratio which is sensitive to a wide range of densities (solid line in Figure 2). However, measurements of the irradiance were uncertain due to the presence of the stronger Fe XX line except in the largest flaring events.

The Fe XXI line at 14.573 is blended with a lower temperature line which is present in the pre-flare spectra. By subtracting out a pre-flare profile from the flare spectra effectively eliminates any contribution from the unidentified feature during the SXR peak of the flare, as any enhancement from lower temperature lines are not thought to be significant until later in the flare (for coronal lines) or during the impulsive phase (for chromospheric lines; see Chamberlin et al. 2012).

Each line ratio has a low and high density limit, beyond which the ratio is not suitable for determining electron densities. The low density limit for each of the ratios was taken to be 10^{11} cm^{-3} .

2.2. Background Subtraction

As some of the Fe lines under investigation are relatively weak, an accurate background subtraction process is crucial for determining the line flux solely due to the flare. Milligan et al. (2012) recently pointed out that the entire MEGS-A wavelength range includes the underlying free-free continuum emission (which is coronal in origin) that becomes enhanced during solar flares, steepening at shorter wavelengths. On top of this lies a pseudo-continuum formed by the close proximity of the many high-temperature Fe lines. However, as the transitions here lie within 2.5 nm of each other, it is reasonable to assume a constant background across all four lines. Therefore, the entire 12-15 nm range was fitted with 17 Gaussian profiles plus a constant background at each time step throughout the flare (see bottom panel of Figure 1).

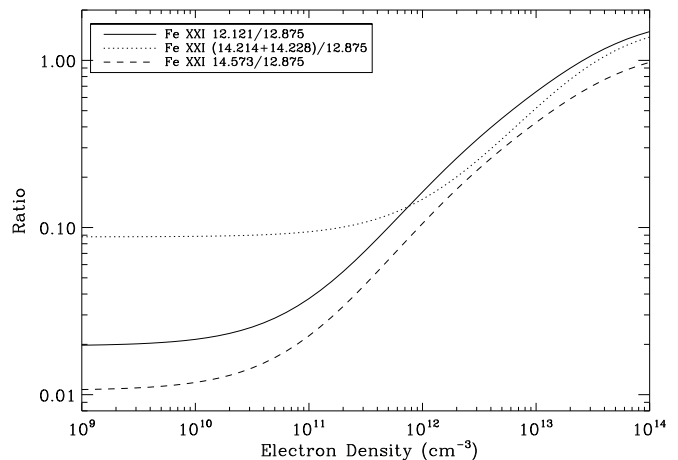


FIG. 2.— Theoretical line ratios for three Fe XXI line pairs calculated using the CHIANTI atomic database.

2.3. Uncertainties

In the current release of the EVE data (level 2, version 2), the uncertainties on the irradiance values have not yet been included and the validation efforts are ongoing. As such, each line profile was fit with a Gaussian profile with constant weighting. To calculate uncertainties in the measured densities, the errors in the line intensities (as derived from the least squares fit of the Gaussian profile) were added in quadrature to give upper and lower limits on the flux ratios. There were then converted into upper and lower limits of the density for each time interval. If the lower limit was found to be less than that of the low density limit for a given line pair, then the lower limit was set equal to 10^{11} cm^{-3} . The electron densities corresponding to these limits then provided the range of likely values for each line pair.

3. RESULTS

The methods described in Section 2 were applied to four X-class flares observed by EVE during 2011 and 2012, including the X6.9 event that occurred on 2011 August 9 which is the largest flare observed by EVE to date. In the GOES X-ray light curve, emission is observed to increase starting at approximately 07:50 UT, and the peak X-ray flux occurs at 08:05 UT. Electron densities for this flare were derived from the three Fe XXI line ratios described in Section 2.1 from approximately 08:02 UT until 08:14 UT, during which the values were above the low density limit of the line ratios. The electron density profiles derived from the three line pairs are shown in panels b–d of Figure 3 (solid lines), where the dotted lines represent the upper and lower limits of the measured density.

Results from each of the line ratios show a similar trend throughout the main phase of the flare. The electron density increases above the low density limit of the line ratios at approximately 08:02 UT and reaches a peak at around 08:05 UT. There is then a slower decline in density, lasting a period of approximately 9 minutes, at which point the density had decreased to a value below the limit of the line ratios. Each of the three line pairs gave consistent peak electron density values of approximately 10^{12} cm^{-3} . The precise values and times of peak N_e for each line pair is listed in Table 1 along

TABLE 1
VALUES AND TIMES OF PEAK ELECTRON DENSITIES AND PEAK EMISSION MEASURES FOR EACH OF THE FLARES PRESENTED IN THIS STUDY.

Flare	Date	14.573/12.875		(14.214+14.228)/12.875		12.121/12.875		Peak GOES EM (10^{49} cm^{-3})	Time of peak GOES EM (UT)
		Peak Log(N_e)	Time of peak N_e	Peak Log(N_e)	Time of peak N_e	Peak Log(N_e)	Time of peak N_e		
X6.9	2011 Aug 9	$11.92^{+0.18}_{-0.26}$	08:05:06 UT	$12.09^{+0.19}_{-0.30}$	08:04:46 UT	$12.01^{+0.30}_{-0.57}$	08:04:46 UT	29.2	08:05:20 UT
X5.4	2012 Mar 7	$11.17^{+0.41}_{-0.17}$	00:28:53 UT	$11.52^{+0.36}_{-0.52}$	00:25:43 UT	-	-	23.4	00:25:43 UT
X2.2	2011 Feb 15	$11.51^{+0.30}_{-0.87}$	01:57:52 UT	$11.69^{+0.33}_{-0.69}$	01:57:42 UT	$11.46^{+0.30}_{-0.86}$	01:57:32 UT	10.1	01:57:42 UT
X2.1	2011 Sep 6	$11.67^{+0.23}_{-0.40}$	22:21:13 UT	$11.89^{+0.14}_{-0.20}$	22:21:33 UT	$11.82^{+0.51}_{-0.82}$	22:21:33 UT	9.9	22:21:07 UT

with their uncertainties. For comparison, the GOES data for each event are also plotted to show the relative timing of the flaring emission (Figure 3a). From the GOES data an emission measure profile can be derived using the methods described in White et al. (2005). The time of peak electron density is in good agreement with the time of peak emission measure as determined independently from GOES observations (08:05:20 UT, also listed in Table 1), as denoted by the vertical dashed line.

This analysis was repeated for three other X-class flares: the X5.4 on 2012 March 7, the X2.2 on 2011 February 15, and X2.1 on 2011 September 6. For all events, consistent peak density values of $10^{11.5}$ – $10^{11.9} \text{ cm}^{-3}$ were obtained from each line pair, although reliable values could not be measured for the X5.4 flare using the 12.121/12.875 ratio (see Table 1), which may have been due to the dominance of the neighbouring Fe XX line. Despite this limitation, time profiles of 5–30 minutes were obtained for each flare.

4. CONCLUSIONS

In this Letter we present techniques for determining time-dependent measurements of the (coronal) electron density using high-temperature ($\sim 12 \text{ MK}$) density-sensitive line ratios during four X-class solar flares. Previous values of electron densities at flare temperatures have only been presented for a small sample of events, at a single time during those flares with integration times of several minutes (Phillips et al. 1983, Mason et al. 1984, Lawson & Peacock 1984). EVE now allows the time profiles of electron densities at flare temperatures to be determined, ultimately, for a statistically significant sample of events throughout the course of solar cycle 24, due to the $\sim 100\%$ duty cycle of EVE.

After investigating many density sensitive line pairs from lines in Fe XIX–Fe XXII, and accounting for blends within the EVE spectral resolution, the most reliable ratios were found to be Fe XXI 12.121/12.875, (14.214+14.228)/12.875, and 14.573/12.875, in agreement with those identified by Mason et al. (1984). Each of these line pairs is sensitive to densities in the range 10^{11} – 10^{14} cm^{-3} . Applying these diagnostics techniques to four X-class flares revealed peak densities of $10^{11.2}$ – $10^{12.1} \text{ cm}^{-3}$, in broad agreement with Mason et al. (1984).

The highest densities measured were for an X6.9 flare and were of the order of 10^{12} cm^{-3} . The fact that consistent values were obtained using each of the line pairs indicate that any potential line blending did not significantly affect the measurements. While comparable values were obtained for the other X-class flares analyzed, no values

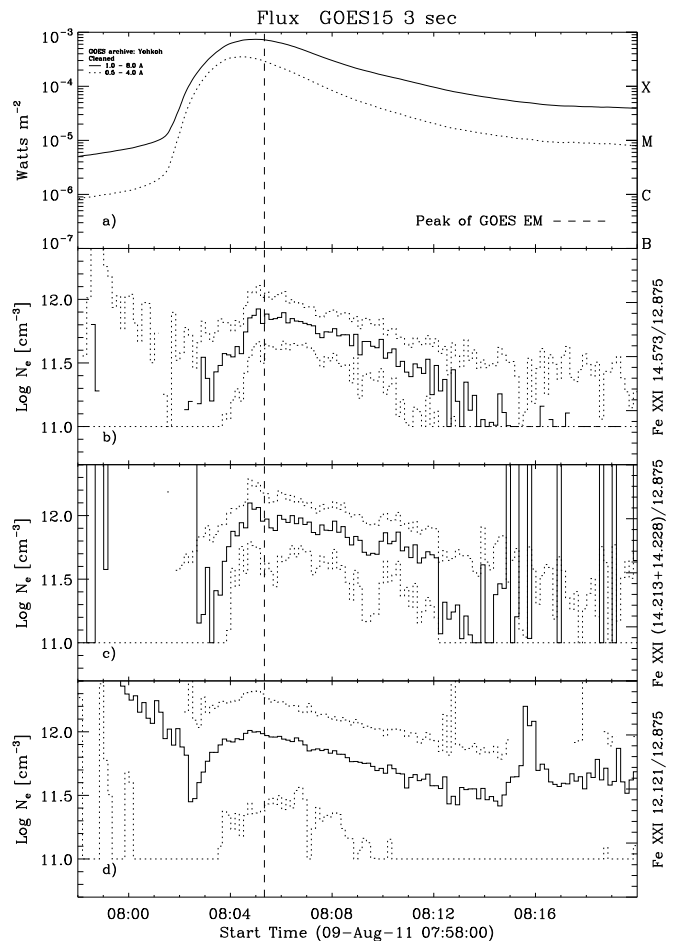


FIG. 3.— Electron density profiles from three Fe XXI line ratios during the X6.9 class flare on 2011 August 9. Panel a shows the GOES lightcurves for the event in the 0.05–0.4 and 0.1–0.8 nm channels. Panels b–d show the time profiles of electron density determined using the 14.573/12.875, (14.214+14.228)/12.875, and 12.121/12.875 Fe XXI ratios, respectively (solid lines). Dotted lines denote the upper and lower density limits. The vertical dashed line in each panel indicates the time of peak emission measure as derived from GOES data.

of electron density above the low density limit could be determined for any M-class flares that were investigated. This limits the suitability of the line ratios investigated to X-class events where the electron density is greater than 10^{11} cm^{-3} , except perhaps in extreme cases. These results tentatively suggest that electron densities are larger in solar flares with a higher peak X-ray flux.

Perhaps more significantly, from the time profiles of the density evolution, the time of maximum density was

found to coincide with that of the peak emission measure as determined from GOES data. The GOES 0.05–0.4 and 0.1–0.8 nm passbands contain strong contributions from highly-ionized iron (the Fe XXV/Fe XX complex at 0.185 nm; White et al. 2005) as well as free-free continuum emission. It is reasonable to assume, therefore, that the X-ray emission observed by GOES would emanate from approximately the same flaring plasma for which the electron densities were derived.

An accurate determination of the electron density is important for understanding both the heating and cooling of flare plasmas, and the mechanisms responsible. For example, the high densities often inferred from the SXR emitting corona during flares are believed to be a result of chromospheric evaporation, whereby chromospheric material is ablated up into the corona by a beam of non-thermal electrons as inferred from blueshifts of high-temperature emission lines (e.g., Antonucci & Dennis 1983, Czaykowska et al. 1999, Milligan & Dennis 2009). Density values are therefore useful for determining the mass rate into (and out of) the overlying loops during evaporation (and condensation). Flare cooling is also believed to be dominated by thermal conduction around the peak of a flare once the injected energy is switched off (e.g., Raftery et al. 2009). This transitions to radiative cooling at some point during the decay phase. As this cooling scales as the square of the electron density inaccurate assumptions of N_e may lead to large inaccuracies in the amount of radiative cooling. Similarly, the amount of energy radiated during a flare can be estimated using GOES data. Recently, Ryan et al. (2012) measured the total radiative losses for $\sim 50,000$ flares as a function of GOES class. A constant density of 10^{10} cm^{-3} was assumed across each event. The results presented here show that large flares can have densities 1–2 orders of magnitude higher, and that that value can vary during individual events. Combining GOES and EVE observations can therefore lead to a more accurate determination of flare energetics.

The volumetric filling factor, f , can also be determined by a combination of imaging and spectroscopy once the density is known. EM can be derived from continuum

observations from GOES or the Ramaty High-Energy Solar Spectroscopic Imager (RHESSI; Lin et al. 2002), while the volume can be estimated from imaging instruments such as RHESSI, GOES/Soft X-ray Imager, Hinode/X-ray Telescope or the Atmospheric Imaging Assembly (AIA) also on SDO, although AIA is known to saturate during the largest flares. High coronal densities may also help explain the occurrence of coronal HXR emission which is believed to be due to electrons accelerated from a coronal reconnection site impinging upon the underlying loop. Previous estimates place this value as low as $10^9\text{--}10^{10} \text{ cm}^{-3}$, although these were often from much weaker events (Krucker et al. 2008). Precise knowledge of the flare loop density can be used to establish whether the observed emission is due to thick- or thin-target bremsstrahlung.

Despite being designed to measure changes in the solar EUV irradiance, several recent studies, in addition to the work presented here, have demonstrated how EVE observations can be used to determine some of the fundamental properties of solar flare plasmas: Woods et al. (2011) presented evidence for a flare ‘late phase’, as well as coronal dimming; Hudson et al. (2011) were able to derive Doppler velocities despite EVE’s modest spectral resolution; Milligan et al. (2012) showed that it is possible to determine the timing and energetics of the free-free and free-bound continuum during large events; and Chamberlin et al. (2012) describes how EVE can be used to measure the thermal evolution of the flaring plasma. Combining these, and other, analyses of solar flares throughout Solar Cycle 24 will give us new insights into their global behaviours and properties.

The authors would like to thank the anonymous referee for their comments which helped improve this manuscript. ROM is grateful to the Leverhulme Trust for financial support from grant F/00203/X, and to NASA for LWS/TR&T grant NNX11AQ53G. He would also like to thank Dr. Phillip Chamberlin for his advice on EVE calibration. MM and FPK acknowledge financial support from the Science and Technology Facilities Council.

REFERENCES

- Antonucci, E., & Dennis, B. R. 1983, *Sol. Phys.*, 86, 67
 Bryans, P., Landi, E., & Savin, D. W. 2009, *ApJ*, 691, 1540
 Chamberlin, P. C., Milligan, R. O., & Woods, T. N. 2012, *Sol. Phys.*, 74
 Culhane, J. L., et al. 2007, *Sol. Phys.*, 243, 19
 Czaykowska, A., de Pontieu, B., Alexander, D., & Rank, G. 1999, *ApJ*, 521, L75
 Dere, K. P., & Cook, J. W. 1979, *ApJ*, 229, 772
 Doschek, G. A., Feldman, U., Landecker, P. B., & McKenzie, D. L. 1981, *ApJ*, 249, 372
 Doschek, G. A., Meekins, J. F., & Cowan, R. D. 1973, *Sol. Phys.*, 29, 125
 Feldman, U., Landi, E., & Doschek, G. A. 2008, *ApJ*, 679, 843
 Feldman, U., Mandelbaum, P., Seely, J. F., Doschek, G. A., & Gursky, H. 1992, *ApJS*, 81, 387
 Gallagher, P. T., Phillips, K. J. H., Lee, J., Keenan, F. P., & Pinfield, D. J. 2001, *ApJ*, 558, 411
 Graham, D. R., Fletcher, L., & Hannah, I. G. 2011, *A&A*, 532, A27
 Hudson, H. S., Woods, T. N., Chamberlin, P. C., Fletcher, L., Del Zanna, G., Didkovsky, L., Labrosse, N., & Graham, D. 2011, *Sol. Phys.*, 273, 69
 Kastner, S. O., Neupert, W. M., & Swartz, M. 1974, *ApJ*, 191, 261
 Krucker, S., et al. 2008, *A&A Rev.*, 16, 155
 Landi, E., Del Zanna, G., Young, P. R., Dere, K. P., & Mason, H. E. 2012, *ApJ*, 744, 99
 Lawson, K. D., & Peacock, N. J. 1984, *A&AS*, 58, 475
 Lin, R. P., et al. 2002, *Sol. Phys.*, 210, 3
 Mason, H. E., Bhatia, A. K., Neupert, W. M., Swartz, M., & Kastner, S. O. 1984, *Sol. Phys.*, 92, 199
 Mason, H. E., Doschek, G. A., Feldman, U., & Bhatia, A. K. 1979, *A&A*, 73, 74
 McKenzie, D. L., Broussard, R. M., Landecker, P. B., Ruge, H. R., Young, R. M., Doschek, G. A., & Feldman, U. 1980, *ApJ*, 238, L43
 Milligan, R. O. 2011, *ApJ*, 740, 70
 Milligan, R. O., Chamberlin, P. C., Hudson, H. S., Woods, T. N., Mathioudakis, M., Fletcher, L., Kowalski, A. F., & Keenan, F. P. 2012, *ApJ*, 748, L14
 Milligan, R. O., & Dennis, B. R. 2009, *ApJ*, 699, 968
 Milligan, R. O., Gallagher, P. T., Mathioudakis, M., Keenan, F. P., & Bloomfield, D. S. 2005, *MNRAS*, 363, 259
 Monsignori Fossi, B. C., Landini, M., Del Zanna, G., & Bowyer, S. 1996, *ApJ*, 466, 427

- Phillips, K. J. H., Bhatia, A. K., Mason, H. E., & Zarro, D. M. 1996, *ApJ*, 466, 549
- Phillips, K. J. H., Feldman, U., & Landi, E. 2008, *Ultraviolet and X-ray Spectroscopy of the Solar Atmosphere* (Cambridge University Press)
- Phillips, K. J. H., Lemen, J. R., Cowan, R. D., Doschek, G. A., & Leibacher, J. W. 1983, *ApJ*, 265, 1120
- Raftery, C. L., Gallagher, P. T., Milligan, R. O., & Klimchuk, J. A. 2009, *A&A*, 494, 1127
- Ryan, D. F., Milligan, R. O., Gallagher, P. T., Dennis, B. R., Tolbert, A. K., Schwartz, R. A., & Young, C. A. 2012, *ApJS*
- Warren, H. P., Feldman, U., & Brown, C. M. 2008, *ApJ*, 685, 1277
- Warren, H. P., & Winebarger, A. R. 2003, *ApJ*, 596, L113
- White, S. M., Thomas, R. J., & Schwartz, R. A. 2005, *Sol. Phys.*, 227, 231
- Woods, T. N., et al. 2010, *Sol. Phys.*, 3
- . 2011, *ApJ*, 739, 59